Irradiation influence on acousto–defect interaction in silicon n^+-p–structure

O. Ya. Olikh,[1, a)] A. M. Gorb,[1] R. G. Chupryna,[1] and O. V. Pristay–Fenenkov[1]
Faculty of Physics, Taras Shevchenko National University of Kyiv, Kyiv 01601, Ukraine

(Dated: 8 August 2017)

Abstract. The effects of 75 MeV boron (B5+) ions and 60 Co gamma radiation on the IV, CV and spectral responses of PIN photodiodes were studied systematically to understand the radiation tolerance of the devices.

Keywords: acousto–defect interaction, silicon, irradiation

I. INTRODUCTION

It has been shown experimentally that ultrasound (US) can effectively interact with defects. US as defect engineering tool has some advantages: (i) locality of the action due to the predominant absorption in regions of deviation in the lattice periodicity; (ii) selectivity of the influence, which is achieved by variation of ultrasonic wave (USW) polarization and type; (iii) possibility of resonance transformations in the defect system due to the oscillation nature of process action. (iv) capability of reversible effect, which is observed in the low intensity USW utilization case.

In the case of piezoelectric semiconductors, the acousto–defect interaction (ADI) is determined mainly by electric field, which accompanies the vibration wave propagation. This effect is expected and is something related to acousto–electric phenomena. But US influence on defect system is also observed in non–piezoelectric crystals like silicon, which is dominant material in microelectronic. Thus it is experimentally observed in silicon crystals and silicon based structures, that US caused an atomic diffusion[1,2], transformed a native and an impurity defect[3–7] modified interior surface states[8–10], created new defect[11,12]. Defects are known to determine a most of semiconductor device properties. And exactly the ADI is a reason of US induced variation of tunneling[13,14], a generation–recombination[15–17] and a thermionic emission[18,19] current in silicon barrier structures.

The main mechanisms of elastic vibration–defect interaction in non-piezoelectric crystals are considered to be the change of population of impurity oscillator levels[20], the displacement of impurity atoms with respect to their surroundings[4,21,22], the decreasing of the diffusion activation energy[23], the local temperature increase by clusters of point defects[24], the dislocation absorption of ultrasound[16,25,26]. However to the best of our knowledge, the complete ADI theory in silicon is absent. One of a top–ranked cause of this situation is a lack of experimental works, which have focused on investigation of acoustically induced (AI) effects.

Not all silicon defects are acoustically active and are subjected to modification under US action. The ADI efficiency depends on the defects centers type and structure[8]. Thus, for example according to[21,22], the force acting on the point defect during US loading (USL) is proportionate to volume elastic strain caused by the relaxation of the defect volume $\Delta\Omega_d$. The irradiation is most widespread and studied methods of alteration of semiconductor defects. On the one hand, it is shown[27–30], that high–power US treatment leads to residual changes of the irradiated silicon structure properties. This effect deals with AI annealing of radiation defects (RDs). On the other hand, irradiation can be a reason of reversible AI phenomenon initiation[31,32], which is caused by formation of acoustically active RDs. Unfortunately, there have only few reports on acoustically driven phenomenon in irradiated silicon structures.

Our goal is to investigate experimentally the AI variations of electrical characteristic which take place in non–irradiated and irradiated n^+-p–Si structures. Irradiation was carried by reactor neutrons and a ^{60}Co–gamma source. It is expected that γ–radiation introduces vacancy–impurity point defects (VO_i complex predominantly)[33–35] whereas neutrons create cluster defects[36,37], disordered regions[38] and C_iO_i complex[35,39] mainly. This work represents distinctions of AI changes in silicon structures with different RDs. The used US intensity (W_{US}) was not very high (< 0.5 W/cm^2) to avoid the irreversible defect subsystem modification, which can be deals with a new defect creation, a RDs annealing or a long distance (a great many interatomic distance) AI diffusion. As a result, the full recovery of n^+-p–Si structure characteristics was observed after the stop of an AW propagation. The models of coupled defect level recombination[40,41], Shockley–Read–Hall (SRH) recombination, and dislocation–induced impedance[42,43] were used to describe the processes in the space charge region, in the diode base, and shunt resistance respectively. The interaction of defects with an inhomogeneous USW

[a)] Electronic mail: olikh@univ.kiev.ua

strain field[21,22] was recruited to explain the observed AI phenomena. The investigation would provide not only better ADI understanding but could also facilitate the development of acoustically controlled devices or radiation sensors.

II. EXPERIMENTAL AND CALCULATION DETAILS

The 2 inch (300 μm thick) p–type boron doped, <111> orientation, Czochralski (Cz) silicon wafer having resistivity of 10 Ω·cm was used for fabrication of n^+-p–Si structure. The n^+ emitter with carrier concentration of about 10^{19} cm^{-3} and thickness of 0.5 μm was formed by phosphorus implantation. Then wafer surface was passivated by Al_2O_3 film and further capped by TiO_x as antireflective coating. Finally the aluminium front (metal grid) and rear (solid contact) electrodes were deposited by screen printing before rapid annealing. The samples with area of about 2 cm^2 used in experiments were cut from the central part of the wafer. 1 sample was irradiated with neutrons in the fluence of $\Psi_n = 4 \cdot 10^{11}$ n/cm^2 and was denoted as nSC. 2 samples were irradiated with ^{60}Co γ–rays in the dose $D_{\gamma 1} = 10^6$ rad and $D_{\gamma 2} = 10^7$ rad and were denoted as g6SC and g7SC respectively. The label iSC was used for non–irradiated sample. To avoid an impact of long–term annealing, which are typical to neutron damaged structure especially[35,36], irradiated samples were stored for 5 years at room temperature before measuring. According to data[44,45] the neutron dose and gamma fluences can be calculated as $D_n = 4.5 \cdot 10^3$ rad and $\Psi_{\gamma 1} = 1.6 \cdot 10^{15}$ γ/cm^2 and $\Psi_{\gamma 2} = 1.6 \cdot 10^{16}$ γ/cm^2 respectively. The non–ionizing energy losses (NIEL) and lifetime damage–constants (K_τ) for neutron differ from γ–^{60}Co ones by four order of magnitude[33,44]: NIEL$_n$ = $2.04 \cdot 10^{-3}$ MeV cm^2/g, NIEL$_\gamma$ = $1.07 \cdot 10^{-7}$ MeV cm^2/g, $K_{\tau,n} = 10^{-7}$ cm^2/s, $K_{\tau,\gamma} = 5 \cdot 10^{-12}$ cm^2/s. Therefore neutrons and γ-rays are expected to produce a similar damage ($\Psi_{\gamma 1} \cdot K_{\tau,\gamma} < \Psi_n \cdot K_{\tau,n} < \Psi_{\gamma 2} \cdot K_{\tau,\gamma}$).

The dark forward current–voltage (I–V) characteristics of the samples both with and without USL were measured over a temperature range 290–340 K. The temperature was controlled by differential copper–constantan thermocouple. Some curves are shown in Fig. 1.

The double–diode model of n^+–p structure I–V characteristics expressed in the following form:

$$I(V,T) = I_{SCR} + I_{base} + I_{sh}\ , \tag{1}$$

$$I_{SCR} = \frac{qAn_i d}{2\tau_g}\left\{\exp\left[\frac{q(V-IR_s)}{n_{\rm id}kT}\right]-1\right\}, \tag{2}$$

$$I_{base} = \frac{qAn_i^2}{p_p}\sqrt{\frac{\mu_n kT}{\tau_n}}\left\{\exp\left[\frac{q(V-IR_s)}{kT}\right]-1\right\}, \tag{3}$$

$$I_{sh} = (V-IR_s)/R_{sh}\,, \tag{4}$$

where I_{SCR} reflects the overall recombination in the space charge region (SCR), I_{base} is closely related to recombination in the quasi-neutral region, I_{sh} is the shunt current, A is the sample area, n_i is the intrinsic carrier concentration, τ_g is the SCR carrier lifetime, d is the SCR thickness:

$$d = \sqrt{\frac{2\varepsilon\varepsilon_0(p_p+n_n)}{q^2 p_p n_n}\left[E_g - kT\ln\left(\frac{N_v N_c}{p_p n_n}\right) - 2kT - Vq\right]}, \tag{5}$$

ε is the permittivity (11.7 for Si), p_p and n_n are the majority carrier concentration in the p– and n–type regions, E_g is the semiconductor band gap, N_c and N_v are the effective density of states in the conduction and valence bands; $n_{\rm id}$ is the ideality factor of the nonideal current components, R_s and R_{sh} are the series and shunt resistances of the structure, μ_n and τ_n are the electron (minority carrier) mobility and lifetime in the diode base.

We used Eqs. (1)–(5) to fit the experimental data and τ_g, τ_n, $n_{\rm id}$, R_{sh}, and R_s were taken as the fittings parameters. The known[46–48] temperature dependencies of n_i, E_g, and μ_n were used. The extremely good fit to the experimental data was obtained — see Fig. 1. In particular, the R_s value 1 Ω was determined for all samples.

In the USL case, the transverse acoustic waves with frequency of 4.2 MHz were exited with help of a piezoelectric transducer and were injected in the samples from the base side in the [111]-direction. The USLs parameters of different samples are listed in the Table I. It was reported previously[6,7,19] that a characteristic time of change in the silicon structure parameters under the ultrasound action did not exceed $2 \cdot 10^3$ s. In order to wait till the acoustically induced (AI) transitional period the following experimental procedure has been used. After USL start the sample was kept at room temperature during 60 min and then the I–V measurements and the sample heating were started. In order to avoid the effect of piezoelectric field on I–V characteristics, the piezoelectric transducer has been shielded.

TABLE I. The parameters of ultrasound loadings.

Sample	W_{US} (W/cm^2)	Label
iSC	0.22	Ui–1
	0.40	Ui–2
nSC	0.21	Un–1
	0.36	Un–2
g6SC	0.32	Ug6–2
g7SC	0.24	Ug7–1
	0.40	Ug7–2

The linear and non-linear fitting were done by using the least-squares and differential evolution[49] method, respectively.

III. RESULTS AND DISCUSSION

A. Space charge region

The I–V characteristics parameters, which deal with SCR phenomena, are $n_{\rm id}$ and τ_g. The finding tempera-

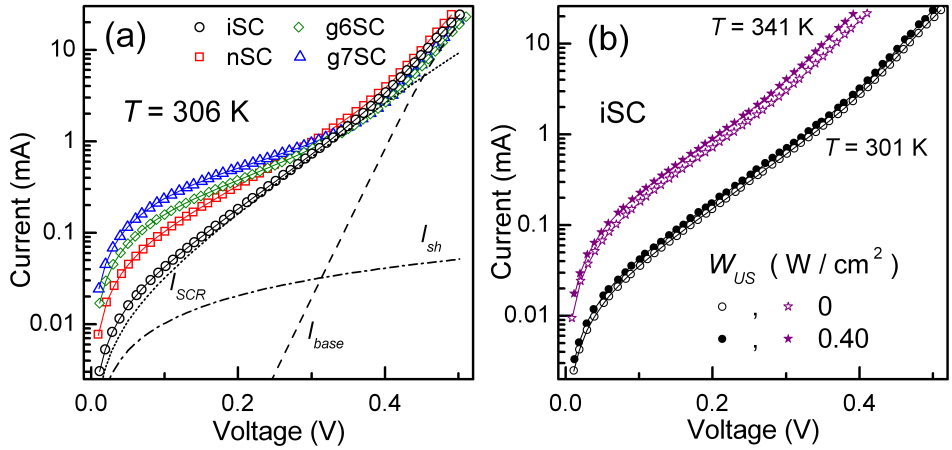

FIG. 1. Dark I–V characteristics measured (a) at 306 K for non–irradiated (circles), neutron–irradiated (squares) and gamma–irradiated (diamonds and triangles) structures without USL; (b) at 301 K (circles) and 341 K (asterisks) with (filled marks, Ui–2) and without (open marks) USL for the iSC. The marks are the experimental results, the solid lines are the fitted curves using Eqs. (1)–(5). The dashed, dot–dashed and dotted lines in (a) are the base, SCR and shunt components of iSC current, respectively.

TABLE II. Characteristics of temperature dependences of n^+-p–Si structure parameters.

Sample	USL	T_0 (K)	$E_{\tau g}$ (eV)
iSC	non	330 ± 30	0.24 ± 0.01
	Ui–1	310 ± 30	0.24 ± 0.01
	Ui–2	360 ± 30	0.24 ± 0.01
nSC	non	1610 ± 70	0.45 ± 0.02
	Un–1	1600 ± 70	0.44 ± 0.02
	Un–2	1680 ± 70	0.44 ± 0.02
g6SC	non	610 ± 40	0.28 ± 0.01
	Ug6–2	1080 ± 50	0.33 ± 0.02
g7SC	non	770 ± 50	0.29 ± 0.01
	Ug7–1	1260 ± 60	0.34 ± 0.02
	Ug7–2	1270 ± 60	0.35 ± 0.02

TABLE III. Acoustically induced change of n^+-p–Si structure parameters (at 330 K).

Sample	USL	$\Delta n_{\rm id}$ (± 0.01)	$\varepsilon_{\tau g}$ ($\pm 5\%$)	$\varepsilon_{\tau r}$ ($\pm 12\%$)	ε_{Rsh} ($\pm 5\%$)
iSC	Ui–1	0.02	-14	-43	-15
	Ui–2	0.03	-17	-58	-32
nSC	Un–1	-0.13	5	-60	-19
	Un–2	-0.26	13	-75	-34
g6SC	Ug6–2	-0.15	2	-67	-3
g7SC	Ug7–1	-0.26	49	-39	-5
	Ug7–2	-0.36	70	-58	-8

ture dependences of ideality factor and SCR lifetime are shown in Fig. 2 and Fig. 3 respectively.

As one can recognize, ideality factor decreases with temperature increase and plots $n_{\rm id}$ vs $1/T$ are close to linear. Thus dependence $n_{\rm id}(T)$ can be expressed as

$$n_{\rm id}(T) = n_{{\rm id},\infty} + T_0/T \, . \qquad (6)$$

On the other hand, the thermoactivated SCR carrier lifetime growth is observed over the explored temperature range - see Fig. 3. The following equation allows to describe sufficiently τ_g temperature dependence:

$$\tau_g(T) = \tau_{g0} \exp\left(-\frac{E_{\tau g}}{kT}\right) \, . \qquad (7)$$

The T_0 and $E_{\tau g}$ values, which were determined for both non-irradiated and irradiated samples with as well as without USL are listed in the Table II.

We want to stress, that (i) irradiation leads to T_0 and $E_{\tau g}$ changes, the g6SC's ideality factor characteristic temperature and SCR lifetime characteristic energy values are closely related to g7SC ones at similar conditions; (ii) USL results in both T_0 and $E_{\tau g}$ increase in γ–irradiated samples — see Fig. 2(b) and Fig. 3(b), but same effect is not observed in non–irradiated and neutron–irradiated samples — see Fig. 2(a) and Fig. 3(a); (iii) USL affects $n_{\rm id}$ and τ_g values, absolute AI changes of ideality factor $\Delta n_{\rm id} = n_{{\rm id},US} - n_{{\rm id},in}$ and relative AI changes of SCR lifetime $\varepsilon_{\tau g} = (\tau_{g,US} - \tau_{g,in})/\tau_{g,in}$ (where subscripts "US" and "in" identify with values, which obtained at the same temperature with and without USL respectively) are listed in the Table III; (iv) Δn and $\varepsilon_{\tau g}$ have an opposite sign for non–irradiated and irradiated samples (for SCg6 not in whole temperature range); (v) ideality factor is varied by USL more effectively in irradiated samples; (vi) US influence efficiency for γ–irradiated samples rises with dose; (vii) AI $n_{\rm id}$ and τ_g changes increase with W_{US} enhancement whereas T_0 and $E_{\tau g}$ values do not depend on ultrasound intensity practically.

For purpose of the present consideration, it is important to discuss an recombination mechanism in the SCR

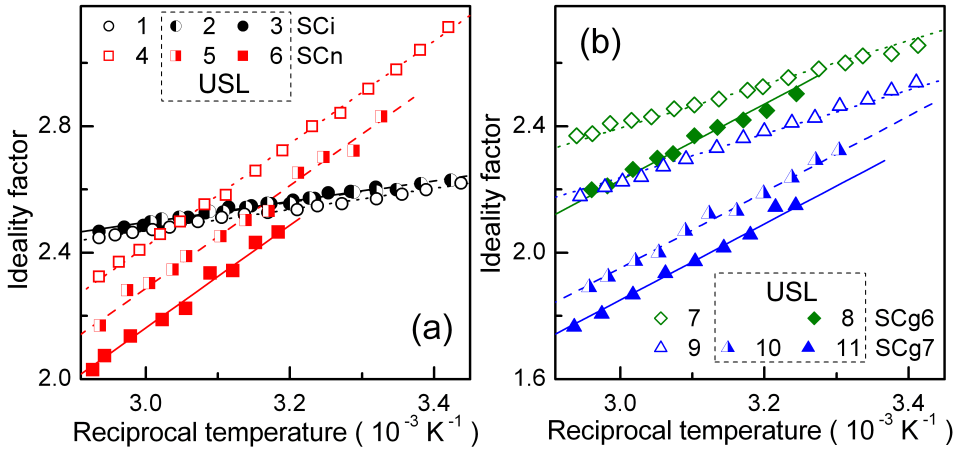

FIG. 2. Temperature dependences of ideality factor for non–irradiated (curves 1–3, circles), neutron–irradiated (4–6, squares) and γ–irradiated (7–11, diamonds and triangles) samples. The curves 1, 4, 7 and 9 (open marks) are obtained without USL, curves 2, 3, 5, 6, 8, 10, and 11 correspond to Ui–1, Ui–2, Un–1, Un–2, Ug6–2, Ug7–1, and Ug7–2 respectively. The marks are the experimental results, the lines are the fitted curves using Eq. (6).

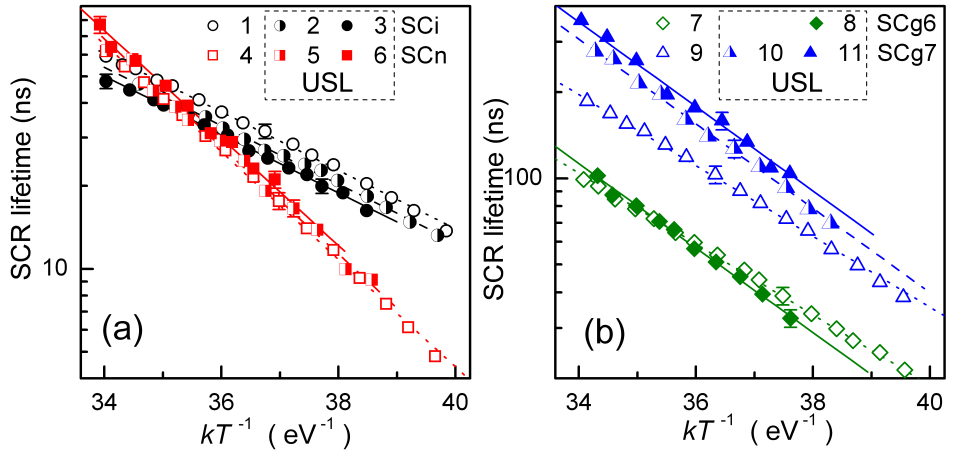

FIG. 3. Temperature dependences of SCR lifetime for non–irradiated (curves 1–3, circles), neutron–irradiated (4–6, squares) and γ–irradiated (7–11, diamonds and triangles) samples. The curves 1, 4, 7 and 9 (open marks) are obtained without USL, curves 2, 3, 5, 6, 8, 10, and 11 correspond to Ui–1, Ui–2, Un–1, Un–2, Ug6–2, Ug7–1, and Ug7–2 respectively. The marks are the experimental results, the lines are the fitted curves using Eq. (7).

of the investigated samples. According to classical SRH theory, an ideality factor must be less than 2 and τ_g temperature dependence is expected[50,51] to be described by the relation $\tau_g \simeq 2\tau_n\sqrt{\sigma_n/\sigma_p}\cosh\left[\left(E_t - E_i\right)/kT\right]$ (where σ_n, σ_p, and E_t are the electron and hole capture cross sections and the energy level of the recombination center, E_i is the intrinsic energy level). In the our case, n_{id} is lager than 2 and τ_g increases with temperature. Therefore SRH theory is inapplicable to the investigated samples. Several attempts to explain large n_{id} have been made with various models[52–55]. But all observed features of SCR recombination (ideality factor large value, independence on light intensity, dependence on temperature as well as carrier lifetime small value and thermoactivated behavior) can be explained by the model of coupled defect level recombination (CDLR)[40,41] only. This model provides a rapid direct charge transfer between defect levels. Such phenomenon have been observed experimentally firstly[56,57] and then it was recruited to explain process in semiconductor diodes[40,41,58].

According to the CDLR model, recombination is the result of carrier exchange between two defect level and crystal bands. In particular, it is proposed[41] that the recombination rate is dominated by sites where an acceptor–like defect is coupled to a donor-like defect. Unfortunately, the functional relation between I–V characteristic parameters and attributes of defects, which take part in CDLR, is not suggested. In the simplified case, when carrier exchanges between the donor level and the conduction band, between the acceptor level and the valence band, and between the donor level and the acceptor level are allowed, the total recombination rate R can be

expressed[40] as

$$R = \frac{R_{12} - \sqrt{R_{12}^2 - 4(np - n_i^2)\tau_{\mathtt{D},n}\tau_{\mathtt{A},p}(1-\epsilon)}}{2\tau_{\mathtt{D},n}\tau_{\mathtt{A},p}(1-\epsilon)}\,, \quad (8)$$

$$R_{12} = \frac{(n+n_{\mathtt{D}})(p+p_{\mathtt{A}})}{R_{\mathtt{DA}}} + \tau_{\mathtt{D},n}(p+p_{\mathtt{D}}) + \tau_{\mathtt{A},p}(n+n_{\mathtt{A}}), \quad (9)$$

$$R = \frac{R_{12} - \sqrt{R_{12}^2 - 4(np - n_i^2)\tau_{\mathtt{D},n}\tau_{\mathtt{A},p}(1-\epsilon)}}{2\tau_{\mathtt{D},n}\tau_{\mathtt{A},p}(1-\epsilon)}\,, \quad (10)$$

$$R_{12} = \frac{(n+n_{\mathtt{D}})(p+p_{\mathtt{A}})}{2\,R_{\mathtt{DA}}\tau_{\mathtt{D},n}\tau_{\mathtt{A},p}(1-\epsilon)} + \frac{\tau_{\mathtt{D},n}(p+p_{\mathtt{D}}) + \tau_{\mathtt{A},p}(n+n_{\mathtt{A}})}{2\tau_{\mathtt{D},n}\tau_{\mathtt{A},p}(1-\epsilon)}, \quad (11)$$

gggggggg
with

$$R_{12} = \left(\frac{(n+n_D)(p+p_A)}{r_{DA}\tau_{D,n}\tau_{A,p}} + \frac{p+p_D}{\tau_{A,p}} + \frac{n+n_A}{\tau_{D,n}}\right)[2(1-\epsilon)]^{-1}. \quad (12)$$

$$R_{12} = \frac{(n+n_{\mathtt{D}})(p+p_{\mathtt{A}})}{R_{\mathtt{DA}}} + \tau_{\mathtt{D},n}(p+p_{\mathtt{D}}) + \tau_{\mathtt{A},p}(n+n_{\mathtt{A}}). \quad (13)$$

$$R_{12} = \frac{(n+n_D)(p+p_A)}{2r_{DA}\tau_{D,n}\tau_{A,p}(1-\epsilon)} + \frac{\tau_{D,n}(p+p_D) + \tau_{A,p}(n+n_A)}{2\tau_{D,n}\tau_{A,p}(1-\epsilon)}. \quad (14)$$

Fig. 4 shows the series resistance over the explored temperature range.

IV. CONCLUSION

In this work, 16 methods were implemented to extract the physical parameters of Schottky diodes. To do so, experimental and synthetic I–V data were used. It has been analyzed the dependences of extraction accuracy of series resistance, barrier height and ideality factor on the parameters value and on the noise level of the I–V curve. It has been shown that the use of Lambert function for numerical calculation allows to reduce both the determination error value and the number of accuracy influencing factor; whereas the running time increases. It has been examined the adaptive procedure, which provide selection of the I–V data range for an auxiliary function construction taking into account the deviation of calculated curve and curve under investigation. This procedure find out to improve the accuracy of analytical Gromov method, especially in the case of low noise level data. In consideration of evolutionary algorithms, the MABC method is favorable over the DE, the PSO and the TLBO due to the minimal running time. The most reliable and preferred methods seem to be evolutionary algorithms (specifically the MABC), Gromov method with adaptive procedure and Lee method. The first one is reasonable in the case of a small R_s value (a few ohms) or a large I_s value (high temperature).

Thus, ultrasound can be an effective tool for controlling silicon structure characteristics.

[1] M. Jivanescu, A. Romanyuk, and A. Stesmans, J. Appl. Phys. **107**, 114307 (2010).
[2] A. Romanyuk, P. Oelhafen, R. Kurps, and V. Melnik, Appl. Phys. Lett. **90**, 013118 (2007).
[3] I. A. Buyanova, S. S. Ostapenko, M. K. Sheinkman, and M. Murrikov, Semicond. Sci. Technol. **9**, 158 (1994).
[4] O. Korotchenkov and H. Grimmliss, Physical Review B **52**, 14598 (1995).
[5] O. Y. Olikh, Semiconductors **43**, 745 (2009).
[6] S. S. Ostapenko and R. E. Bell, Journal of Applied Physics **77**, 5458 (1995).
[7] I. Ostrovskii, O. Korotchenkov, O. Olikh, A. Podolyan, R. Chupryna, and M. Torres-Cisneros, J. Opt. A: Pure Appl. Opt. **3**, S82 (2001).
[8] D. Kropman, V. Seeman, S. Dolgov, and A. Medvids, phys. stat. sol. (c) **13**, 793 (2016).
[9] N. Zaveryukhina, E. Zaveryukhina, S. Vlasov, and B. Zaveryukhin, Technical Physics Letters **34**, 241 (2008).
[10] S. A. Mirsagatov, I. B. Sapaeva, and Z. Nazarov, Inorganic Materials **51**, 1 (2015).
[11] R. Savkina, A. Smirnov, T. Kryshtab, and A. Kryvko, Mater. Sci. Semicond. Process. **37**, 179 (2015).
[12] M. Virot, R. Pflieger, E. V. Skorb, J. Ravaux, T. Zemb, and H. Mohwald, J. Phys. Chem. C **119**, 15493 (2012).
[13] O. Y. Olikh, K. V. Voytenko, R. M. Burbelo, and J. M. Olikh, Journal of Semiconductors **37**, 122002 (2016).
[14] O. Olikh, Semiconductors **45**, 798 (2011).
[15] A. Davletova and S. Z. Karazhanov, Journal of Physics and Chemistry of Solids **70**, 989 (2009).
[16] A. Davletova and S. Z. Karazhanov, Journal of Physics D: Applied Physics **41**, 165107 (2008).
[17] V. Melnik, Y. Olikh, V. Popov, B. Romanyuk, Y. Goltvyanskii, and A. Evtukh, Materials Science & Engineering, B: Solid-State Materials for Advanced Technology **124–125**, 327 (2005).
[18] O. Y. Olikh, K. V. Voytenko, and R. M. Burbelo, Journal of Applied Physics **117**, 044505 (2015).
[19] O. Olikh, Ultrasonics **56**, 545 (2015).
[20] V. N. Pavlovich, phys. stat. sol. (b) **180**, 97 (1993).
[21] F. Mirzade, J. Appl. Phys. **110**, 064906 (2011).
[22] R. Peleshchak, O. Kuzyk, and O. Dan'kiv, Ukr. J. Phys. **61**, 741 (2016).
[23] V. D. Krevchik, R. A. Muminov, and A. Y. Yafasov, phys. stat. sol. (a) **63**, K159 (1981).
[24] F. Mirzade, J. Appl. Phys. **97**, 084911 (2005).
[25] I. Ostrovskii and O. Korotchenkov, Solid State Commun. **82**, 267 (1992).
[26] O. Olikh and K. Voytenko, Ultrasonics **66**, 1 (2016).
[27] N. Guseynov, Y. Olikh, and S. Askerov, Tech. Phys. Lett. **33**, 18 (2007).
[28] P. Parchinskii, S. Vlasov, and L. Ligai, Semiconductors **40**, 808 (2006).
[29] A. Gorb, O. Korotchenkov, O. Olikh, and A. Podolian, IEEE Trans. Nucl. Sci. **57**, 1632 (2010).
[30] A. O. Podolian, A. B. Nadtochiy, and O. A. Korotchenkov, Tech. Phys. Lett. **38**, 405 (2012).
[31] Y. Olikh, M. Tymochko, and A. Dolgolenko, Tech. Phys. Lett. **32**, 586 (2006).
[32] Y. Olikh and M. Tymochko, Tech. Phys. Lett. **37**, 37 (2011).
[33] H. Jafari and S. Feghhi, Nucl. Instrum. Methods Phys. Res., Sect. A **816**, 62 (2016).
[34] Y. P. Rao, K. Praveen, Y. R. Rani, A. Tripathi, and A. G. Prakash, Nucl. Instrum. Methods Phys. Res., Sect. B **316**, 205 (2013).
[35] M. Moll, H. Feick, E. Fretwurst, G. Lindström, and C. Schütze, Nucl. Instrum. Methods Phys. Res., Sect. A **388**, 335 (1997).
[36] J. Srour, C. Marshall, and P. Marshall, IEEE Trans. Nucl. Sci. **50**, 653 (2003).
[37] I. Pintilie, G. Lindstroem, A. Junkes, and E. Fretwurst, Nucl. Instrum. Methods Phys. Res., Sect. A **611**, 52 (2009).
[38] N. Arutyunov, N. Bennett, N. Wight, R. Krause-Rehberg,

V. Emtsev, N. Abrosimov, and V. Kozlovski, phys. stat. sol. (b) **253**, 2175 (2016).
[39] C. A. Londos, G. Antonaras, and A. Chroneos, J. Appl. Phys. **114**, 193513 (2013).
[40] A. Schenka and U. Krumbein, Journal of Applied Physics **78**, 3185 (1995).
[41] S. Steingrube, O. Breitenstein, K. Ramspeck, S. Glunz, A. Schenk, and P. P. Altermatt, Journal of Applied Physics **110**, 014515 (2011).
[42] V. Gopal and S. Gupta, IEEE Trans. Electron Devices **50**, 1220 (2003).
[43] V. Gopal and S. Gupta, IEEE Trans. Electron Devices **51**, 1078 (2004).
[44] A. Akkerman, J. Barak, M. Chadwick, J. Levinson, M. Murat, and Y. Lifshitz, Radiat Phys Chem **62**, 301 (2001).
[45] D. Bräunig and F. Wulf, Radiat. Phys. Chem. **43**, 105 (1994).
[46] A. B. Sproul and M. A. Green, J. Appl. Phys. **73**, 1214 (1993).
[47] D. K. Schroder, *Semiconductor Material and Device Characterization*, 3rd ed. (John Wiley & Sons, New Jersey, 2006).
[48] A. McEvoy, T. Markvart, and L. Castaner, eds., *Solar Cells. Materials, Manufacture and Operation*, 2nd ed. (Academic Press, Oxford, 2013).
[49] K. Wang and M. Ye, Solid-State Electron. **53**, 234 (2009).
[50] D. Schroder, IEEE Trans. Electron Devices **29**, 1336 (1982).
[51] H. Aharoni, T. Ohmi, M. M. Oka, A. Nakada, and Y. Tamai, J. Appl. Phys. **81**, 1270 (1997).
[52] A. S. H. van der Heide, A. Schonecker, J. H. Bultman, and W. C. Sinke, Progress in Photovoltaics: Research and Applications **13**, 3 (2005).
[53] J. Beier and B. Voss, in *Proceedings of the 23rd IEEE Photovoltaic Specialists Conference* (1993) pp. 321–326, Louisville, KY, USA.
[54] J. M. Shah, Y.-L. Li, T. Gessmann, and E. F. Schubert, J. Appl. Phys. **94**, 2627 (2003).
[55] A. Kaminski, J. J. Marchand, H. E. Omari, A. Laugier, Q. N. Le, and D. Sarti, in *Proceedings of the 25th IEEE Photovoltaic Specialists Conference* (1996) pp. 573–576, Washington, DC, USA.
[56] W. M. Chen, B. Monemar, E. Janzén, and J. L. Lindström, Phys. Rev. Lett. **67**, 1914 (1991).
[57] A. M. Frens, M. T. Bennebroek, A. Zakrzewski, J. Schmidt, W. M. Chen, E. Janzén, J. L. Lindström, and B. Monemar, Phys. Rev. Lett. **72**, 2939 (1994).
[58] O. Breitenstein, J. Bauer, P. P. Altermatt, and K. Ramspeck, Solid State Phenomena **156–158**, 1 (2010).